Multimode Strong Coupling in Cavity Optomechanics

P. Kharel,[1,2,*,‡] Y. Chu,[1,2,3,4,‡] D. Mason,[1,2] E. A. Kittlaus,[1,2] N. T. Otterstrom,[1,2] S. Gertler,[1,2] and
P. T. Rakich[1,2,†]

[1]*Department of Applied Physics, Yale University, New Haven, Connecticut 06511, USA*
[2]*Yale Quantum Institute, Yale University, New Haven, Connecticut 06520, USA*
[3]*Department of Physics, ETH Zürich, Zürich 8093, Switzerland*
[4]*Quantum Center, ETH Zürich, Zürich 8093, Switzerland*

Optomechanical systems show great potential as quantum transducers and information storage devices for use in future hybrid quantum networks. In this context, optomechanical strong coupling can enable efficient, high-bandwidth, and deterministic transfer of quantum states. While optomechanical strong coupling has been realized at optical frequencies, it has proven difficult to identify a robust optomechanical system that features the low loss and high coupling rates required for more sophisticated control of mechanical motion. In this paper, we demonstrate strong coupling in a Brillouin-based bulk cavity optomechanical system in both the single-mode and the multimode strong-coupling regime, which leads to a useful device both for applications in quantum information and for investigating decoherence phenomena in bulk acoustic wave resonators. Using nontrivial mode hybridizations in the strong-coupling regime, we create hybridized photonic-phononic modes with lifetimes that are significantly longer than those of the uncoupled system. This surprising lifetime enhancement, which results from the interference of decay channels, showcases the use of multimode strong coupling as a general strategy to control extrinsic decoherence mechanisms. Moreover, phonons supported by such bulk-acoustic-wave resonators have a collection of properties, including high frequencies, long coherence times, and robustness against thermal decoherence, that make this optomechanical system particularly enticing for applications such as quantum transduction and memories. Hence, this system provides access to phenomena in a previously unexplored regime of optomechanical interactions and could serve as an important building block for future quantum devices.

I. INTRODUCTION

As is the case for many quantum optical systems, optomechanical devices exhibit different physical behaviors and acquire useful capabilities when they enter the so-called strong-coupling regime [1]. In this regime, the coupling rate between light and motion becomes faster than both the optical and the mechanical dissipation rates, which is necessary for applications such as quantum transduction [2,3] and memories [4,5]. Since light is the natural carrier of quantum information over long distances [6], and mechanical motion couples efficiently to many quantum systems [7–9], a robust and coherent interface between light and mechanical motion could be a useful building block in hybrid quantum networks for long-distance communications [10] or for modular quantum computation

[11]. In such systems, strong coupling permits operation in a regime where the transduction bandwidth can be maximized. Beyond quantum communication, strong coupling is also necessary for applications that seek to utilize information stored in an optical mode [12] rather than that released from a cavity, such as in hybrid quantum systems where light is coupled to individual atoms or quantum dots [13,14].

Only a few optomechanical devices have entered the regime of optomechanical strong coupling, due to technical challenges associated with realizing low-loss systems that can also robustly support high coupling rates. Radiation pressure has been used to achieve strong coupling between terahertz-frequency optical modes and megahertz-frequency mechanical modes in micromechanical systems [15,16]. However, if we seek to utilize optomechanical systems as a quantum resource, it is advantageous to instead utilize high-frequency (gigahertz) phonon modes; this is because higher frequencies yield lower thermal decoherence at any given temperature,

---

*prashanta.kharel@gmail.com
†peter.rakich@yale.edu
‡These two authors contributed equally.

024054-1

enable faster quantum operations, and allow access to the mechanical ground state using standard refrigeration techniques. Despite the many successes of gigahertz-frequency micro- and nano-optomechanical systems [17], it remains challenging to reach strong coupling in such systems, due to practical limits [18,19] on the circulating photon number, which in turn limit the cavity-enhanced coupling rate.

In an alternative approach, Brillouin interactions have been used to demonstrate strong coupling to gigahertz-frequency mechanical modes of a fused-silica whispering-gallery-mode resonator [20]. This strategy permits resonant driving of the optical mode, and the use of macroscopic fused-silica-based resonators having low material- and surface-induced absorption alleviates some of the technical challenges associated with laser heating, making large coupling rates more readily accessible. While this recent demonstration illustrates the advantages of Brillouin-based coupling in macroscopic systems, low acoustic dissipation rates-necessary to store information in mechanical modes-are difficult to achieve in glasses at cryogenic temperatures. In particular, two-level tunneling-state systems, which are intrinsic to silica, produce excess dissipation and noise at cryogenic temperatures [21,22], complicating the prospects for efficient quantum operations in such systems. However, a promising way to address this challenge could be to realize strong coupling between optical-cavity modes and long-lived high-frequency (greater than 10 GHz) phonon modes supported by crystalline bulk-acoustic-wave (BAW) resonators [23].

Separate from the opportunities presented by strong coupling, another direction with significant untapped potential in cavity optomechanics—and, more generally, in quantum information science—involves the exploration of coupled multimode systems. Such systems have already given rise to the observation of a wide variety of interesting physical phenomena, such as optomechanical dark modes [24,25], synchronization of mechanical frequencies [26], topological dynamics [27], and nonreciprocity [28]. Achieving strong coupling in a multimode system could lead to a wealth of capabilities, including storage of light through control of bright and dark states [29], and the exploration of topological phonon transport [30,31]. Furthermore, in the quantum regime, multimode strong coupling could open the door to the generation of multipartite mechanical entanglement [32–34] and the implementation of a quantum simulator for many-body bosonic systems [35,36].

In this paper, we utilize Brillouin interactions to demonstrate strong coupling between a single optical mode and one or more high-frequency (12.6 GHz) modes of a crystalline bulk acoustic resonator at cryogenic temperatures. Our system combines a high-finesse optical resonator with a low-loss crystalline BAW resonator, which can be reconfigured so that the optical mode is strongly coupled to either a single acoustic mode or several acoustic modes.

Using both frequency- and time-domain measurements, we quantify the parameters of the system and explore its dynamics. In the single-mode case, we achieve an optomechanical coupling rate $g_m = 2\pi \times (7.2 \pm 0.1)$ MHz, which exceeds both the optical dissipation rate $\kappa = 2\pi \times (4.43 \pm 0.02)$ MHz and the mechanical dissipation rate $\Gamma_m = 2\pi \times (66 \pm 3)$ kHz. In the multimode case, the coupling rates exceed the acoustic free spectral range $\delta = 2\pi \times (610 \pm 10)$ kHz, meaning that we enter the multimode strong-coupling regime. In this regime, strong coupling produces a set of optomechanical "dark modes" with linewidths that are a factor of 5 less than the smallest dissipation rate, Γ_m, of the uncoupled system. We show that this intriguing phenomenon can be explained by the destructive interference of radiative loss channels for the dark modes.

II. CAVITY OPTOMECHANICAL SYSTEM

Our optomechanical system consists of a planar quartz crystal that is placed within a Fabry-Pérot optical cavity with high-reflectivity (99.9%) optical mirrors [Fig. 1(a)]. At a temperature of approximately 10 K, long-lived longitudinal acoustic modes in the quartz crystal are reflected from the planar surfaces of the crystal to form a series of macroscopic standing-wave acoustic modes similar to the standing-wave electromagnetic modes formed within a Fabry-Perot optical cavity. A high-frequency acoustic mode within the BAW resonator (formed by the quartz crystal) can mediate coupling between two distinct longitudinal modes of the optical cavity through Brillouin interactions when energy-conservation and phase-matching requirements are satisfied [Fig. 1(b)]. For crystalline z-cut quartz at cryogenic temperatures and optical modes near 1550 nm, such interactions occur for a narrow band of acoustic modes near 12.6 GHz (see Supplemental Material Sec. I [38]).

This multimode coupling can be described by the interaction Hamiltonian

$$H_{\text{int}} = -\sum_m \hbar g_0^m (a_2^\dagger a_1 b_m + a_1^\dagger a_2 b_m^\dagger), \qquad (1)$$

where $a_1^\dagger$ ($a_2^\dagger$) is the creation operator for an optical mode at frequency ω_1 (ω_2), $b_m^\dagger$ is the creation operator for an acoustic mode at frequency Ω_m, and g_0^m is the zero-point coupling rate. We note that g_0^m depends on the spatial acousto-optical overlap, which provides us with a way of tailoring the optomechanical coupling strength for different acoustic modes [37]. With an external control laser that is driven on resonance with the lower-frequency optical mode a_1, we can write an effective linearized Hamiltonian as

$$H_{\text{eff}} = \hbar\Delta a_2^\dagger a_2 + \sum_m \hbar\Omega_m b_m^\dagger b_m - \sum_m \hbar g_m (a_2^\dagger b_m + a_2 b_m^\dagger).$$
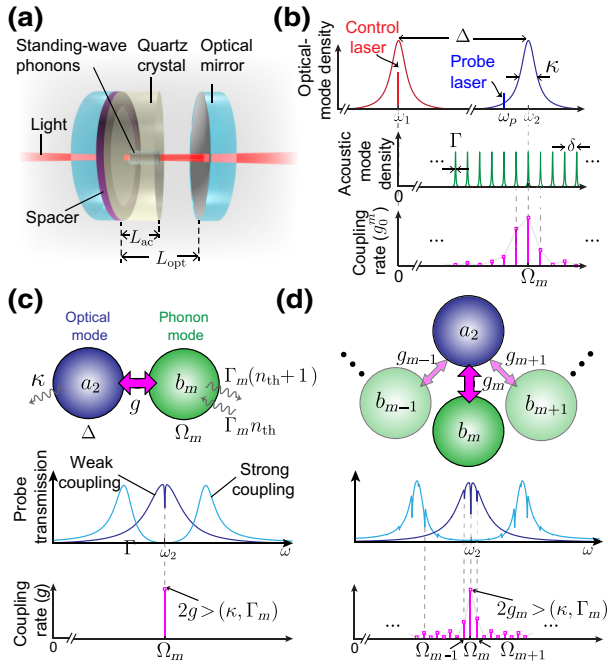
$$(2)$$

FIG. 1. Multimode cavity optomechanical system. (a) Schematic illustration of the optomechanical system (not to scale). The thickness of the half-inch-diameter quartz crystal is $L_{ac} = 5$ mm, and the spacing between the optical mirrors is $L_{opt} = 9.9$ mm. The diameters of the waists of the optical and acoustic modes are 122 and 86 μm, respectively. (b) Schematic spectra of optical modes (top) and acoustic modes (middle). The zero-point optomechanical coupling rates (bottom) are determined by a combination of the Brillouin bandwidth dictated by energy and momentum conservation, and the spatial overlap of acoustic and optical modes [37]. (c) Diagram of linearized optomechanical coupling between an optical mode and a single acoustic mode (top), corresponding to the expected spectra of the probe-laser transmission in the weak- and strong-coupling regimes (middle), and coupling rate under a strong control-laser drive (bottom). (d) As in (c), except that the optical mode is coupled to many acoustic modes. Here, the coupling to one acoustic mode is dominant, corresponding to the case shown in Figs. 2 and 3.

Here, we move to the rotating frame of mode a_1, $g_m = \sqrt{\bar{n}_c} g_0^m$ is the cavity-enhanced coupling rate, $\bar{n}_c$ is the intracavity photon number for mode a_1, and $\Delta = \omega_2 - \omega_1$ is the optical free spectral range.

The above beam-splitter Hamiltonian $\hbar g_m(a_2^\dagger b_m + a_2 b_m^\dagger)$ describes coherent energy exchange between a single optical mode a_2 and a single acoustic mode b_m with an interaction rate $2g_m$. However, the dissipation rates relative to this interaction rate determine the optical transmission spectrum for mode a_2, which we measure using a weak probe field. In the weak-coupling regime $g_m < (\kappa/2, \Gamma_m/2)$, we expect a narrow dip in the transmission spectrum due to the well-known phenomenon of optomechanically induced transparency (OMIT) [39], seen in

Fig. 1(c). In the strong-coupling regime $g_m > (\kappa/2, \Gamma_m/2)$, the optical transmission spectrum develops two resonant features that correspond to new modes that result from the hybridization between the optical mode a_2 and the individual mechanical mode b_m seen in Fig. 1(c).

Because our experimental system permits coupling to an array of acoustic modes, the optical-mode spectrum develops additional features in the strong-coupling regime. Since a BAW resonator supports multiple acoustic modes with a regular frequency spacing (δ) that is smaller than the optical dissipation rate (κ), it is important to go beyond the minimal model of a single optical mode coupled to a single phonon mode. This is because more than one acoustic mode can simultaneously mediate coupling between the same pair of optical modes [Fig. 1(b)]. Therefore, in addition to normal-mode splitting of a single strongly coupled acoustic mode (Ω_m), we expect several OMIT dips to arise from weak coupling to a multitude of acoustic modes (e.g., $\Omega_{m-2}, \Omega_{m-1}, \Omega_{m+1}, \Omega_{m+2}$), as seen in Fig. 1(d).

III. EXPERIMENTAL RESULTS

A. Strong coupling to a single acoustic mode

We first present experimental measurements of strong optomechanical coupling when our system is configured to couple predominantly to a single acoustic mode. For the lowest control-laser power, the transmission spectrum seen in Fig. 2(a)(i) reveals a single OMIT dip at $\Omega_m = 2\pi \times 12.591$ GHz. Through these low-power measurements in the weak-coupling regime, we extract $\kappa = 2\pi \times (4.43 \pm 0.02)$ MHz, $\Gamma_m = 2\pi \times (66 \pm 3)$ kHz, and $g_0^m = 2\pi \times (23 \pm 1)$ Hz (see Supplemental Material Sec. II [38]). Note that the asymmetric line shape seen in Fig. 2(a)(i) is characteristic of leaky modes supported by flat-flat resonator geometries (see Supplemental Material Sec. V.A [38]). To reach the regime of strong coupling, we enhance g_m by increasing $\bar{n}_c$. As expected from theory, we observe a normal-mode splitting that increases in proportion to $\sqrt{P_{in}}$ [Fig. 2(a)], where P_{in} is the input control-laser power.

As another unambiguous signature of strong coupling, we tune the free spectral range of the optical-cavity modes into and out of resonance with the strongly coupled acoustic mode to reveal a characteristic anticrossing feature [Fig. 2(b)]. Because the optical-mode spacing, Δ, depends on the temperature, T, we can readily tune Δ to match the frequency, Ω_m, of the Brillouin-active phonon modes. During these measurements, we lock the control laser on resonance with the optical mode at ω_1, such that temperature tuning allows us to change the optical-mode spacing Δ without changing g_m. From transmission spectra obtained as a function of T at the highest control power, we observe a clear anticrossing at $T = 7.6$ K when $\Delta \simeq \Omega_m$ [Fig. 2(b)(i)]. For the off-resonant case ($\Delta \neq \Omega_m$) at $T = 12.4$ K, we obtain a narrow and a broad resonance feature, seen
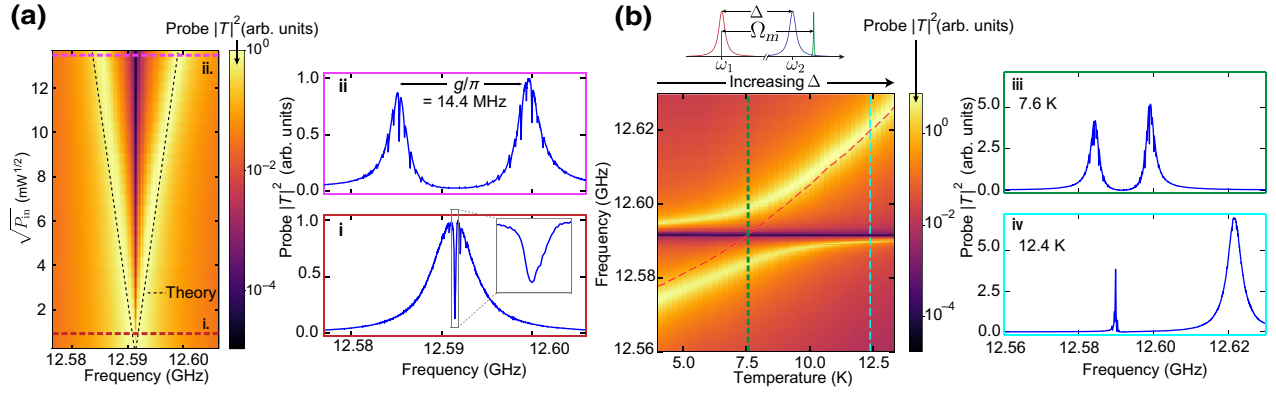
FIG. 2. Optomechanical strong coupling to a single mechanical mode. (a) Probe-laser transmission spectra taken at various control-laser powers. The dashed lines show expected values of g_m for the dominantly coupled acoustic mode, extrapolated from fits to low-power spectra with $\sqrt{P_{in}} < 0.6$ mW$^{1/2}$ (see Supplemental Material Sec. II [38]). The insets (i) and (ii) show spectra in the regimes of strong and weak coupling, respectively. In the strongly coupled case, the normal-mode splitting indicated is due to the dominantly coupled acoustic mode, but OMIT features from other acoustic modes that are still weakly coupled are visible. (b) Probe transmission taken at various cryostat temperatures. The dashed red line shows the value of Δ at each temperature, obtained by fitting the data to a theoretical expression for the probe transmission (see Supplemental Material Sec. II [38]). The insets (iii) and (iv) show spectra in the resonant and far-detuned cases.

in Fig. 2(b)(ii), which correspond to the acoustic and the optical modes, respectively, of the uncoupled system.

At the highest P_{in} of 187 mW, corresponding to an intra-cavity photon number $\bar{n}_c = 1.1 \times 10^{11}$, we observe a splitting $2g_m = 2\pi \times (14.4 \pm 0.1)$ MHz [Fig. 2(a)(ii)]. Since $2g_m/\kappa \simeq 3$ and $2g_m/\Gamma_m \simeq 220$, the coherent coupling rate far exceeds the dissipation rates of both the optical and the acoustic modes, indicating that our system is in the strong-coupling regime. For mechanical oscillators with nonzero thermal occupation, it is relevant to consider not only how the coupling rate compares with the dissipation rates, but also how it compares with the total (thermal) decoherence rate, $\gamma_{th} = n_{th}\Gamma_m$. In this way, one can define the quantum cooperativity, $C_q = 4g_m^2/\kappa\gamma_{th}$. Achieving $C_q > 1$ indicates that quantum state transfer between photons and phonons can occur at a much faster rate than the mechanical deco-herence. This opens the door to many quantum coherent protocols, including efficient and low-noise quantum trans-duction of information between the optical and acoustic domains [40,41].

To characterize γ_{th} (and thus C_q), one must measure the mechanical bath occupation, which we accomplish through a series of calibrated thermometry measurements of undriven thermal motion. By carefully characteriz-ing our optical detection path with an optical calibration tone, and extracting optomechanical scattering rates with a driven measurement, we can reliably calibrate measured rf voltage spectra with respect to units of mechanical quanta necessary to extract the effective phonon occupation num-ber (see Supplemental Material Sec. III for details [38]). From these measurements, we extract a thermal bath occu-pation $n_{th} = 25 \pm 1$, yielding a thermal decoherence rate of $2\pi \times (1.6 \pm 0.1)$ MHz.

To apply standard methods for estimation of the thermal occupation (including the effects of sideband cooling) [42], it is necessary to perform measurements of thermal occu-pation at lower coupling rates. However, to understand the prospects for reaching high quantum cooperativities, we must investigate the possibility of spurious mode heating at higher powers (and higher coupling rates). Absorbed light has been observed to cause excessive heating of the mechanical mode [18,41], limiting the performance of state-of-the-art quantum optomechanical experiments [2,43]. By comparison, the present bulk crystalline sys-tem has several properties that could prove advantageous in this regard. For example, the high-purity quartz crys-tals used in our optomechanical system have exceedingly low material absorption [44]. At the same time, the macro-scopic crystalline substrate has a high thermal conductivity (greater than 20 W cm^{-1} K^{-1}), which peaks around 10 K [45], and also has good thermal anchoring to the cryostat, helping to minimize any temperature changes produced by any deposited heat. To quantify the degree of possible laser heating, we repeat our calibrated thermometry exper-iments in the presence of an auxiliary "heating laser" that is used to drive a separate optical mode (not participating in the optomechanical process). Within the uncertainty of our measurements, we observe that the presence of a strong heating laser does not alter the thermal decoherence rate of the mechanical mode at input optical powers of 150 mW, which is comparable with the highest control-laser pow-ers used to demonstrate strong coupling (see Supplemental Material Sec. III for details [38]).

These measurements confirm that we can reach optome-chanical scattering rates ($4g_m^2/\kappa$) that exceed the thermal decoherence rate (γ_{th}) by over an order of magnitude,

corresponding to the regime of strong quantum cooperativity (or $C_q > 1$). With the parameters demonstrated here, ground-state sideband-cooling experiments should be straightforward, although one must carefully manage and model the multimode interactions and coupled dissipation channels. In this direction, it may be more straightforward to work with a planoconvex crystal [23], which offers a higher acoustic finesse, such that multimode interactions are less relevant.

Next we demonstrate time-domain control and utilize it to study the dynamics of our system under a pulsed probe signal. These pulsed operations not only are an important step toward implementing deterministic state transfer for quantum transduction and information storage, but also allow us to perform accurate measurements of the timescales for coherent and dissipative dynamics in our optomechanical system [41]. We probe the time-domain dynamics of our system by pulsing weak probe light (ω_2) while maintaining a strong continuous drive at ω_1 [Fig. 3(a)]. A heterodyne signal resulting from interference between the control and the probe light transmitted through the cavity provides phase-sensitive detection of the probe light as a function of time (see Supplemental Material Sec. I [38]).
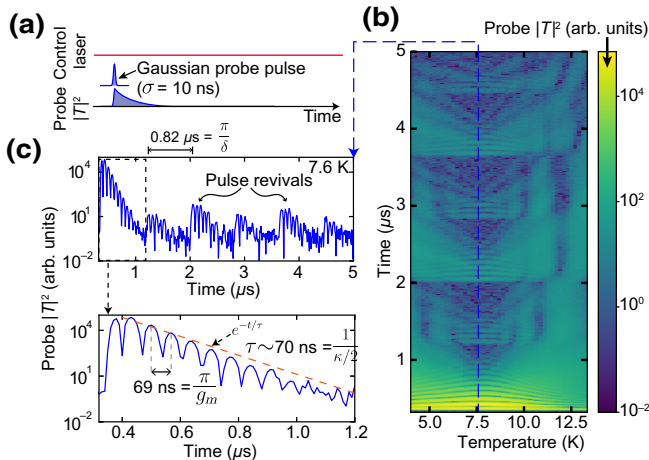

FIG. 3. Time-domain measurements of strong coupling. (a) Schematic illustration of the time-domain measurement. A strong control laser is continuously on resonance with the optical mode at ω_1 to turn on the optomechanical coupling [see Fig. 1(b)]. A short probe pulse excites the optical mode at $\omega_2 = \omega_1 + \Omega_m$, and the response of the system is then recorded as a function of time (see Supplemental Material Sec. I [38]). (b) Time-domain measurements taken at the same set of cryostat temperatures as in Fig. 2(b). Note that in these measurements, the probe frequency is centered at Ω_m but has a large enough bandwidth to excite the optical mode even when it is detuned. (c) Probe transmission as a function of time after the probe pulse is turned on (top), and enlargement (bottom) showing oscillations at π/g_m and exponential decay with timescale $\tau \sim 2/\kappa$.

The temporal response observed using this method helps to elucidate some subtle features that emerge from multimode strong coupling. The time-domain measurements shown in Fig. 3(b) are performed at the same temperatures as for the frequency-domain measurements shown in Fig. 2(b), and result in a characteristic detuning dependency of the Rabi oscillations obtained when two resonators coherently exchange energy in the strong-coupling regime [46]. At $T = 7.6$ K (when $\Delta \simeq \Omega_m$), we observe coherent oscillations with a period of 69 ns, which is consistent with the value of $2g_m$ extracted from frequency-domain measurements. As seen in Fig. 3(c), the time constant τ for the energy decay is 70 ns, which agrees well with the energy decay rate $(\kappa + \Gamma_m)/2 \approx \kappa/2$ of the hybridized modes. Notice, however, that additional revivals of the coherent oscillations are observed for $t \gg \tau$ in Fig. 3(c). These nontrivial features appear because the spectrally broad probe pulse excites a single strongly coupled acoustic mode, as well as a multitude of weakly coupled acoustic modes that lie outside the phase-matching bandwidth. These results are consistent with multiple OMIT dips that arise from weak coupling to multiple acoustic modes in the spectral domain, as seen in Fig. 2(a). Because of the modulation in the coupling strength produced by the overlap between optical and acoustic modes in this device geometry, g_0^m is suppressed for alternating acoustic mode numbers m outside the phase-matching bandwidth [Fig. 1(d)]. For this reason, the observed revivals have a period of 0.82 μs, corresponding to a frequency of 1.2 MHz, which is approximately twice the acoustic free spectral range of 610 kHz. Since the lifetimes of such weakly coupled modes approach the intrinsic mechanical decay time of the uncoupled system, $1/\Gamma_m \simeq 2.4$ μs, the revivals are sustained for $t \gg \tau$.

B. Strong coupling to multiple acoustic modes

So far, we have demonstrated robust strong coupling between a single optical mode and a single high-frequency acoustic mode in our Brillouin-based bulk cavity optomechanical system. Next, we show that this system can be reconfigured to achieve a multimode strong-coupling regime, which leads to useful device physics both for applications in quantum information and for investigating decoherence phenomena in bulk acoustic resonators. To enter the multimode strong-coupling regime, we strongly couple a single optical mode to three acoustic modes [Fig. 4(a)]. We accomplish this by tuning the optical wavelength to select a different pair of optical modes, which changes the spatial overlap between the optical and acoustic modes (see Supplemental Material Sec. I [38]). A transmission spectrum taken at low power [Fig. 4(b)(i)] reveals three OMIT dips. As before, theoretical fits to the OMIT spectrum at low power allow us to extract coupling rates $g_1 = 2\pi \times (4.9 \pm 0.1)$ MHz, $g_2 = 2\pi \times (4.0 \pm 0.1)$
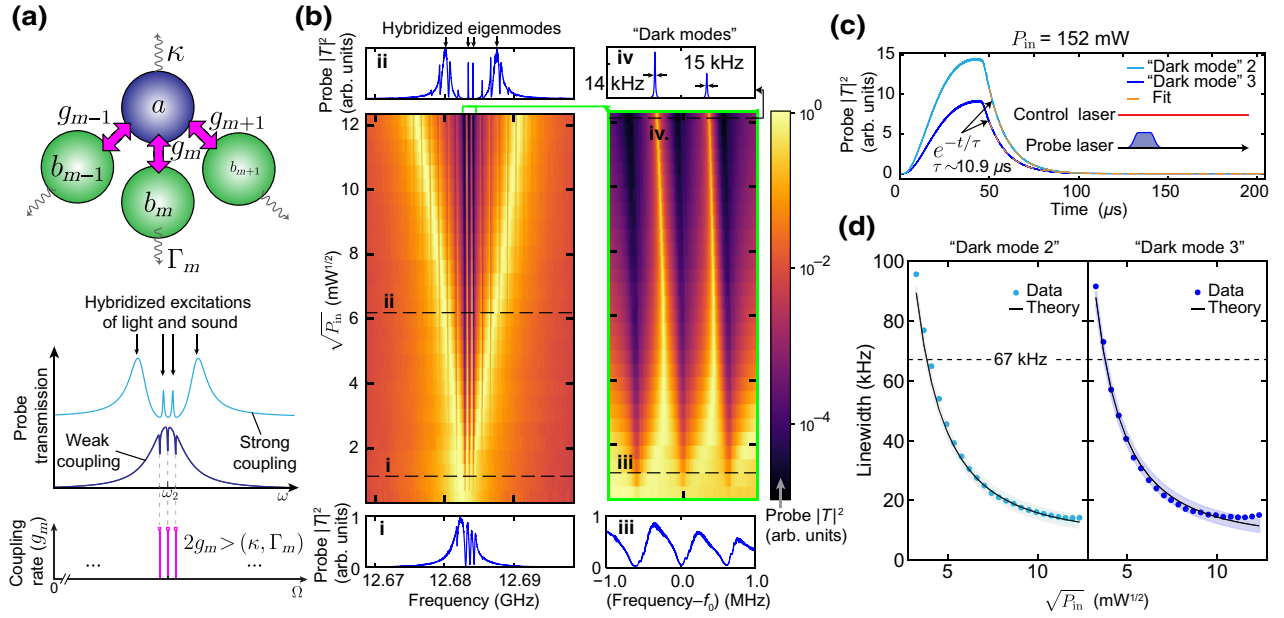
FIG. 4.   Optomechanical strong coupling to three mechanical modes. (a) Diagram of linearized optomechanical coupling between an optical mode and three acoustic modes (top), corresponding expected spectra of the probe-laser transmission in the weak- and strong-coupling regimes (middle), and coupling rate under a strong laser drive (bottom). Strong coupling between an optical mode and three acoustic modes gives rise to four hybridized excitations of light and sound, with two narrow resonances corresponding to optical "dark" modes and two broad resonances corresponding to optical "bright" modes. (b) Probe-laser transmission spectra taken at various P_{in}. The right panel shows an enlargement of these spectra around the frequency $f_0 = 12.684$ GHz. The lower and upper panels [insets (i)–(iv)] show spectra in the regimes of weak and strong coupling, respectively. In the strongly coupled case [insets (ii) and (iv)], two narrow resonances are observed, corresponding to the optomechanical dark modes. (c) Time-domain measurement of dark modes. The inset shows the pulse sequence for the control and probe lasers. (d) Measured linewidth of the two dark modes at various control-laser powers, and fits to theory with $\Gamma_{int}/2\pi = 5$ kHz as described in the main text. The shaded region corresponds to the theoretically predicted linewidth of the two dark modes when we vary the fit parameter $\Gamma_{int}/2\pi$ from 3 to 7 kHz.

MHz, and $g_3 = 2\pi \times (3.7 \pm 0.1)$ MHz, as well as dissipation rates $\kappa = 2\pi \times (2.52 \pm 0.08)$ MHz and $\Gamma_m = 2\pi \times (67 \pm 10)$ kHz (see Supplemental Material Sec. II [38]). In the strong-coupling regime, we observe four distinct peaks in the transmission spectrum, seen in Fig. 4(b)(ii). These peaks represent the four eigenmodes produced by hybridization of the optical mode (a_2) with the three dominant phonon modes b_1, b_2, and b_3.

To understand the nature of these four new eigenmodes, we start by considering a simpler case, of a single optical mode (a_2) coupled strongly to two phonon modes (b_1, b_2) separated by 2δ. Furthermore, we assume that $g_1 = g_2 \equiv g$, $\Gamma_1 = \Gamma_2 \equiv \Gamma$, and $\Omega_{1,2} = \Delta \mp \delta$. The Hamiltonian of this three-coupled-oscillator system in the basis of a_2, b_1, and b_2 is given by

$$H_{eff} = \begin{bmatrix} \Delta - i\kappa/2 & -g & -g \\ -g^* & \Omega_1 - i\Gamma/2 & 0 \\ -g^* & 0 & \Omega_2 - i\Gamma/2 \end{bmatrix}. \quad (3)$$

This effective Hamiltonian can be diagonalized to obtain three eigenmodes of the hybridized system (see Supplemental Material Sec. V [38]). In the limit of large

g, these eigenmodes become two "bright" modes $B_\pm = (1/\sqrt{2})a_2 \pm (1/\sqrt{2})(b_1 + b_2)$ at frequencies $\omega_\pm = \Delta \pm \sqrt{2}g$, with dissipation rates $\kappa_\pm = \kappa/2$, and one "dark" mode $D = (1/\sqrt{2})(b_1 - b_2)$ at a frequency $\omega_D = \Delta$, with a dissipation rate $\kappa_D = \Gamma$. Notice that the bright modes are formed from the superposition of both the optical and the acoustic modes, whereas the dark mode lacks an optical-mode component, meaning that it does not couple to light. The dynamics of such a system, and the existence of such bright and dark modes, has been explored in an electromechanical system using a gigahertz-frequency microwave resonator strongly coupled to two megahertz-frequency micromechanical oscillators [29]. However, this regime of coupling has not been previously accessible for optomechanical systems.

Extending the Hamiltonian in Eq. (3) to treat the case of a single optical mode coupling to three acoustic modes, we now expect four eigenmodes of the hybridized system, as seen in Fig. 4(a). Of these eigenmodes, the two broad peaks correspond to the bright modes, whereas the two narrow peaks correspond to the dark modes. This analysis leads us to expect the decay rates of these dark modes to approach the mechanical decay rate $\Gamma_m = 2\pi \times 67$ kHz.

However, high-resolution measurements of such modes at the highest control-laser powers [seen in Fig. 4(b)(iv)] reveal decay rates $\Gamma_{d2} = 2\pi \times 14$ kHz and $\Gamma_{d3} = 2\pi \times 15$ kHz, which are approximately 5 times smaller than the original acoustic dissipation rate Γ_m. In other words, spectral measurements suggest that the new dark modes formed as a result of strong coupling have much longer lifetimes than any of the uncoupled modes of the system.

To determine the veracity of this counterintuitive result, we perform time-domain ring-down measurements to quantify the lifetime of these dark modes [Fig. 4(c)]. The measured decay time $\tau_d \sim 10.9$ μs confirms that both of these eigenmodes, which are hybridized excitations of both light and sound, have lifetimes that are significantly longer than the optical and mechanical lifetimes of the uncoupled system.

The observed dissipation-reduction phenomenon can be understood as a form of coherent cancellation that occurs when mechanical modes—which couple into a common reservoir—become strongly hybridized. To understand this, we note that that the Brillouin-active phonon modes supported by this crystal structure can be viewed as leaky modes that lose energy through coupling (or radiation) to a band of phonon modes within the flat-flat crystal geometry. Hence, it is natural to decompose the total decay rate (Γ) into distinct radiative (Γ_{rad}) and intrinsic (Γ_{int}) contributions, such that $\Gamma = \Gamma_{rad} + \Gamma_{int}$. Importantly, this radiation constitutes a common bath, and hence Γ_{rad} will appear as both a decay term and a dissipative coupling [47,48] between different mechanical modes (see Supplemental Material Sec. V [38]). In the simple case of two acoustic modes treated above, this corresponds to the addition of an off-diagonal term $-i\Gamma_{rad}$ linking modes b_1 and b_2.

In this case, the resulting decay rate of the dark mode D becomes $\kappa_D = (\Gamma - \Gamma_{rad}) + \kappa\delta^2/2g^2$. If radiative loss was the only decay channel, we would thus find $\kappa_D \to 0$ as g becomes large. In reality, $\kappa_D \to \Gamma_{int}$, the value of which may be set by surface scattering and absorption due to imperfections in the crystal. At cryogenic temperatures, Γ_{int} can be very small in pristine crystals [23,49], opening up the possibility of extremely long-lived dark modes. We note that analogous line-narrowing phenomena due to interference of decay pathways has been investigated in fluorescence spectra of a V-type atomic system [50] and in a circuit-quantum-electrodynamics platform [51].

A measurement of the linewidths of the two dark modes as a function of power [Fig. 4(d)] agrees well with the theoretical description of our system presented above. Theoretical fits to the data, for the case of three phonon modes, are performed by numerically diagonalizing an effective Hamiltonian that includes the radiative coupling terms. Only $\Gamma_{int} = 2\pi \times 5$ kHz is taken as a fit parameter (see Supplemental Material Sec. V [38]), and this is consistent with independent measurements of acoustic damping in quartz crystals at cryogenic temperatures [23,52]. Note

that we observe a larger than expected linewidth of the dark modes at the highest power, which could be due to a deviation from the linear dependence of g on $\sqrt{P_{in}}$ (see Supplemental Material Sec. III [38]). Nevertheless, these experiments clearly demonstrate that, through the formation of hybridized modes, multimode strong coupling becomes a powerful tool to dynamically manipulate decoherence pathways in optomechanical systems.

IV. DISCUSSION

These results demonstrate that optomechanical coupling to a multitude of high-frequency low-loss phonons in a BAW resonator presents intriguing opportunities for investigating classical and quantum phenomena in the multimode strong-coupling regime. Moreover, the time-domain measurements presented in this paper represent an important step toward optical control of bulk acoustic phonons for quantum transduction and the generation of nonclassical mechanical states. While our system is already in the quantum coherent strong-coupling regime necessary to observe quantum effects, a number of improvements can be made to achieve robust quantum control of phonons and realize the aforementioned goals.

First, it is possible to directly initialize such high-frequency (12.6 GHz) phonons in their quantum ground states at temperatures less than 1 K by using a standard dilution refrigerator. Decreasing κ by improving the mirror reflectivity to 99.99% and utilizing low-loss crystalline substrates with a larger Brillouin gain (such as TeO$_2$) could enable access to the strong-coupling regime at input powers less than 100 μW. These improvements, along with low-duty-cycle pulsed operation of the control laser with a microwatt average power, could make operation in dilution refrigerators feasible. More importantly, it would be beneficial to design a fiber-coupled optical-cavity system with a piezotunable crystal position to minimize stray optical reflections, as well as to provide enhanced control over coupling to one or more phonon modes.

These improvements could offer avenues for utilizing multimode optomechanical interactions in future applications of quantum information and metrology. For instance, it may be possible to adiabatically transfer quantum optical states, such as single photons, to long-lived dark states for quantum information storage. Moreover, it may be possible to use nontrivial mode hybridization to generate entangled mechanical states of the resonator by simultaneously swapping optical excitations with multiple strongly coupled acoustic modes [53]. In addition, as shown by the line-narrowing phenomena that we observe, strong coupling between light and acoustic modes in BAW resonators could be used to explore and mitigate acoustic dissipation mechanisms. More generally, it has been shown that acoustic waves in BAW resonators couple strongly

to a variety of other quantum systems, such as superconducting qubits [54], defect centers [55], and microwave fields [9]. Therefore, deterministic control of bulk acoustic waves using light in the strong-coupling regime could be a valuable tool for manipulating quantum information and exploring physical phenomena in hybrid quantum systems.

All data needed to evaluate the conclusions in this paper are present in the paper and/or the Supplemental Material. Additional data are available from the authors upon request.

[1] M. Aspelmeyer, T. J. Kippenberg, and F. Marquardt, Cavity optomechanics, Rev. Mod. Phys. **86,** 1391 (2014).

[2] M. Mirhosseini, A. Sipahigil, M. Kalaee, and O. Painter, Superconducting qubit to optical photon transduction, Nature **588,** 599 (2020).

[3] R. D. Delaney, M. D. Urmey, S. Mittal, B. M. Brubaker, J. M. Kindem, P. S. Burns, C. A. Regal, and K. W. Lehnert, Superconducting-qubit readout via low-backaction electro-optic transduction, Nature **606,** 489 (2022).

[4] V. Fiore, Y. Yang, M. C. Kuzyk, R. Barbour, L. Tian, and H. Wang, Storing Optical Information as a Mechanical Excitation in a Silica Optomechanical Resonator, Phys. Rev. Lett. **107,** 133601 (2011).

[5] K. Stannigel, P. Komar, S. Habraken, S. Bennett, M. D. Lukin, P. Zoller, and P. Rabl, Optomechanical Quantum Information Processing with Photons and Phonons, Phys. Rev. Lett. **109,** 013603 (2012).

[6] H. J. Kimble, The quantum internet, Nature **453,** 1023 (2008).

[7] P. Rabl, P. Cappellaro, M. G. Dutt, L. Jiang, J. Maze, and M. D. Lukin, Strong magnetic coupling between an electronic spin qubit and a mechanical resonator, Phys. Rev. B **79,** 041302 (2009).

[8] A. D. O'Connell, M. Hofheinz, M. Ansmann, R. C. Bialczak, M. Lenander, E. Lucero, M. Neeley, D. Sank, H. Wang, and M. Weides, *et al.*, Quantum ground state and single-phonon control of a mechanical resonator, Nature **464,** 697 (2010).

[9] X. Han, C.-L. Zou, and H. X. Tang, Multimode Strong Coupling in Superconducting Cavity Piezoelectromechanics, Phys. Rev. Lett. **117,** 123603 (2016).

[10] K. Stannigel, P. Rabl, A. S. Sørensen, P. Zoller, and M. D. Lukin, Optomechanical Transducers for Long-Distance Quantum Communication, Phys. Rev. Lett. **105,** 220501 (2010).

[11] K. Lee, B. Sussman, M. Sprague, P. Michelberger, K. Reim, J. Nunn, N. Langford, P. Bustard, D. Jaksch, and I. Walmsley, Macroscopic non-classical states and terahertz quantum processing in room-temperature diamond, Nat. Photonics **6,** 41 (2012).

[12] Y.-D. Wang and A. A. Clerk, Using Interference for High Fidelity Quantum State Transfer in Optomechanics, Phys. Rev. Lett. **108,** 153603 (2012).

[13] K. Hammerer, M. Wallquist, C. Genes, M. Ludwig, F. Marquardt, P. Treutlein, P. Zoller, J. Ye, and H. J. Kimble, Strong Coupling of a Mechanical Oscillator and a Single Atom, Phys. Rev. Lett. **103,** 063005 (2009).

[14] J. P. Reithmaier, G. Sek, A. Löffler, C. Hofmann, S. Kuhn, S. Reitzenstein, L. Keldysh, V. Kulakovskii, T. Reinecke, and A. Forchel, Strong coupling in a single quantum dot–semiconductor microcavity system, Nature **432,** 197 (2004).

[15] S. Gröblacher, K. Hammerer, M. R. Vanner, and M. Aspelmeyer, Observation of strong coupling between a micromechanical resonator and an optical cavity field, Nature **460,** 724 (2009).

[16] E. Verhagen, S. Deléglise, S. Weis, A. Schliesser, and T. J. Kippenberg, Quantum-coherent coupling of a mechanical oscillator to an optical cavity mode, Nature **482,** 63 (2012).

[17] M. Eichenfield, J. Chan, R. M. Camacho, K. J. Vahala, and O. Painter, Optomechanical crystals, Nature **462,** 78 (2009).

[18] J. Chan, T. M. Alegre, A. H. Safavi-Naeini, J. T. Hill, A. Krause, S. Gröblacher, M. Aspelmeyer, and O. Painter, Laser cooling of a nanomechanical oscillator into its quantum ground state, Nature **478,** 89 (2011).

[19] R. Riedinger, S. Hong, R. A. Norte, J. A. Slater, J. Shang, A. G. Krause, V. Anant, M. Aspelmeyer, and S. Gröblacher, Non-classical correlations between single photons and phonons from a mechanical oscillator, Nature **530,** 313 (2016).

[20] G. Enzian, M. Szczykulska, J. Silver, L. Del Bino, S. Zhang, I. A. Walmsley, P. Del'Haye, and M. R. Vanner, Observation of Brillouin optomechanical strong coupling with an 11 GHz mechanical mode, Optica **6**, 7 (2019).

[21] S. Hunklinger and W. Arnold, Ultrasonic properties of glasses at low temperatures, Phys. Acoust. **12**, 155 (1976).

[22] O. Arcizet, R. Rivière, A. Schliesser, G. Anetsberger, and T. J. Kippenberg, Cryogenic properties of optomechanical silica microcavities, Phys. Rev. A **80**, 021803 (2009).

[23] W. Renninger, P. Kharel, R. Behunin, and P. Rakich, Bulk crystalline optomechanics, Nat. Phys. **14**, 601 (2018).

[24] Q. Lin, J. Rosenberg, D. Chang, R. Camacho, M. Eichenfield, K. J. Vahala, and O. Painter, Coherent mixing of mechanical excitations in nano-optomechanical structures, Nat. Photonics **4**, 236 (2010).

[25] C. Dong, V. Fiore, M. C. Kuzyk, and H. Wang, Optomechanical dark mode, Science **338**, 1609 (2012).

[26] G. Heinrich, M. Ludwig, J. Qian, B. Kubala, and F. Marquardt, Collective Dynamics in Optomechanical Arrays, Phys. Rev. Lett. **107**, 043603 (2011).

[27] H. Xu, D. Mason, L. Jiang, and J. Harris, Topological energy transfer in an optomechanical system with exceptional points, Nature **537**, 80 (2016).

[28] F. Ruesink, M.-A. Miri, A. Alu, and E. Verhagen, Nonreciprocity and magnetic-free isolation based on optomechanical interactions, Nat. Commun. **7**, 13662 (2016).

[29] F. Massel, S. U. Cho, J.-M. Pirkkalainen, P. J. Hakonen, T. T. Heikkilä, and M. A. Sillanpää, Multimode circuit optomechanics near the quantum limit, Nat. Commun. **3**, 987 (2012).

[30] V. Peano, C. Brendel, M. Schmidt, and F. Marquardt, Topological Phases of Sound and Light, Phys. Rev. X **5**, 031011 (2015).

[31] H. Xu, L. Jiang, A. A. Clerk, and J. G. E. Harris, Nonreciprocal control and cooling of phonon modes in an optomechanical system, Nature **568**, 65 (2019).

[32] M. J. Weaver, D. Newsom, F. Luna, W. Löffler, and D. Bouwmeester, Phonon interferometry for measuring quantum decoherence, Phys. Rev. A **97**, 063832 (2018).

[33] L. M. D. Lépinay, C. F. Ockeloen-Korppi, M. J. Woolley, and M. A. Sillanpää, Quantum mechanics–free subsystem with mechanical oscillators, Science **372**, 625 (2021).

[34] S. Kotler, G. A. Peterson, E. Shojaee, F. Lecocq, K. Cicak, A. Kwiatkowski, S. Geller, S. Glancy, E. Knill, R. W. Simmonds, J. Aumentado, and J. D. Teufel, Direct observation of deterministic macroscopic entanglement, Science **372**, 622 (2021).

[35] M. Ludwig and F. Marquardt, Quantum Many-Body Dynamics in Optomechanical Arrays, Phys. Rev. Lett. **111**, 073603 (2013).

[36] M. J. Hartmann, Quantum simulation with interacting photons, J. Opt. **18**, 104005 (2016).

[37] P. Kharel, G. I. Harris, E. A. Kittlaus, W. H. Renninger, N. T. Otterstrom, J. G. Harris, and P. T. Rakich, High-frequency cavity optomechanics using bulk acoustic phonons, Sci. Adv. **5**, 1 (2019).

[38] See Supplemental Material at http://link.aps.org/supplemental/10.1103/PhysRevApplied.18.024054 for additional experimental details, and Refs. [56–61].

[39] S. Weis, R. Rivière, S. Deléglise, E. Gavartin, O. Arcizet, A. Schliesser, and T. J. Kippenberg, Optomechanically induced transparency, Science **330**, 1520 (2010).

[40] A. H. Safavi-Naeini, D. Van Thourhout, R. Baets, and R. Van Laer, Controlling phonons and photons at the wavelength scale: Integrated photonics meets integrated phononics, Optica **6**, 213 (2019).

[41] S. M. Meenehan, J. D. Cohen, G. S. MacCabe, F. Marsili, M. D. Shaw, and O. Painter, Pulsed Excitation Dynamics of an Optomechanical Crystal Resonator near Its Quantum Ground State of Motion, Phys. Rev. X **5**, 041002 (2015).

[42] A. H. Safavi-Naeini, J. Chan, J. T. Hill, S. Gröblacher, H. Miao, Y. Chen, M. Aspelmeyer, and O. Painter, Laser noise in cavity-optomechanical cooling and thermometry, New J. Phys. **15**, 035007 (2013).

[43] R. Riedinger, A. Wallucks, I. Marinković, C. Löschnauer, M. Aspelmeyer, S. Hong, and S. Gröblacher, Remote quantum entanglement between two micromechanical oscillators, Nature **556**, 473 (2018).

[44] D. Pinnow and T. Rich, Development of a calorimetric method for making precision optical absorption measurements, Appl. Opt. **12**, 984 (1973).

[45] R. Zeller and R. Pohl, Thermal conductivity and specific heat of noncrystalline solids, Phys. Rev. B **4**, 2029 (1971).

[46] Y. Chu, P. Kharel, W. H. Renninger, L. D. Burkhart, L. Frunzio, P. T. Rakich, and R. J. Schoelkopf, Quantum acoustics with superconducting qubits, Science **358**, 199 (2017).

[47] A. Metelmann and A. A. Clerk, Nonreciprocal Photon Transmission and Amplification via Reservoir Engineering, Phys. Rev. X **5**, 021025 (2015).

[48] K. Fang, J. Luo, A. Metelmann, M. H. Matheny, F. Marquardt, A. A. Clerk, and O. Painter, Generalized nonreciprocity in an optomechanical circuit via synthetic magnetism and reservoir engineering, Nat. Phys. **13**, 465 (2017).

[49] S. Galliou, M. Goryachev, R. Bourquin, P. Abbé, J. P. Aubry, and M. E. Tobar, Extremely low loss phonon-trapping cryogenic acoustic cavities for future physical experiments, Sci. Rep. **3**, 2132 (2013).

[50] P. Zhou and S. Swain, Quantum interference in resonance fluorescence for a driven V atom, Phys. Rev. A **56**, 3011 (1997).

[51] N. M. Sundaresan, Y. Liu, D. Sadri, L. J. Szőcs, D. L. Underwood, M. Malekakhlagh, H. E. Türeci, and A. A. Houck, Beyond Strong Coupling in a Multimode Cavity, Phys. Rev. X **5**, 021035 (2015).

[52] P. Kharel, Y. Chu, M. Power, W. H. Renninger, R. J. Schoelkopf, and P. T. Rakich, Ultra-high-Q phononic resonators on-chip at cryogenic temperatures, APL Photonics **3**, 066101 (2018).

[53] M. J. Weaver, F. Buters, F. Luna, H. Eerkens, K. Heeck, S. de Man, and D. Bouwmeester, Coherent optomechanical state transfer between disparate mechanical resonators, Nat. Commun. **8**, 824 (2017).

[54] Y. Chu, P. Kharel, T. Yoon, L. Frunzio, P. T. Rakich, and R. J. Schoelkopf, Creation and control of multi-phonon Fock

states in a bulk acoustic-wave resonator, Nature **563**, 666 (2018).

[55] E. MacQuarrie, T. Gosavi, A. Moehle, N. Jungwirth, S. Bhave, and G. Fuchs, Coherent control of a nitrogen-vacancy center spin ensemble with a diamond mechanical resonator, Optica **2**, 233 (2015).

[56] D. F. Walls and G. J. Milburn, *Quantum Optics* (Springer Science & Business Media, Springer, Berlin, Heidelberg, 2007).

[57] F. Marquardt, J. P. Chen, A. A. Clerk, and S. M. Girvin, Quantum Theory of Cavity-Assisted Sideband Cooling of Mechanical Motion, Phys. Rev. Lett. **99**, 093902 (2007).

[58] H. J. Carmichael, Quantum Trajectory Theory for Cascaded Open Systems, Phys. Rev. Lett. **70**, 2273 (1993).

[59] A. A. Clerk, M. H. Devoret, S. M. Girvin, F. Marquardt, and R. J. Schoelkopf, Introduction to quantum noise, measurement, and amplification, Rev. Mod. Phys. **82**, 1155 (2010).

[60] D. Cardimona, M. Raymer, and C. Stroud Jr., Steady-state quantum interference in resonance fluorescence, J. Phys. B: At., Mol. Phys. **15**, 55 (1982).

[61] E. Nichelatti and G. Salvetti, Spatial and spectral response of a Fabry–Perot interferometer illuminated by a Gaussian beam, Appl. Opt. **34**, 4703 (1995).